

# Nacre morphology and chemical composition in Atlantic winged oyster *Pteria colymbus* (Röding, 1798)

Pablo Santana and Dalila Aldana Aranda

Departamento de Recursos del Mar, Centro de Investigación y de Estudios Avanzados del Instituto Politécnico Nacional, Mérida, Yucatán, México

## ABSTRACT

The microstructure and nanostructure of nacre in *Pteria colymbus* were studied with high-resolution field emission scanning electron microscopy (FESEM). The tablets were found to be flat and polyhedral with four to eight sides, and lengths ranging from 0.6 to 3.0  $\mu\text{m}$ . They consisted of nanocrystals 41 nm wide, growing in the same direction. X-ray diffraction showed the crystals to be mineral phase aragonite, which was confirmed by Raman spectroscopy. Fourier transform infrared spectroscopy identified a band at  $1,786.95\text{ cm}^{-1}$  attributed to carboxylate (carbonyl) groups of the proteins present in the organic matrix as well as bands characteristic of calcium carbonate. X-ray fluorescence showed the nacre to contain 98% calcium carbonate, as well as minor elements (Si, Na, S and Sr) and trace elements (Mg, P, Cu, Al, Fe, Cl, K and Zn).

**Subjects** Aquaculture, Fisheries and Fish Science, Biochemistry, Marine Biology, Aquatic and Marine Chemistry

**Keywords** Nacre, Microstructure, Nanocrystals, Oyster, Chemical composition, Pteria

## INTRODUCTION

Mollusk shells are mineralized tissues that fulfill structural functions (*Addadi, Raz & Weiner, 2003*). In all three main mollusk classes (Cephalopoda, Gastropoda and Bivalvia) the shell consists of stratified layers, each with a unique mineral composition (*Dauphin & Denis, 2000*). Shell-forming crystals are organized on these layers according to different configurations which define a shell's microstructures. Specific microstructures are characteristic of calcite (i.e., prismatic, foliate) and aragonite (i.e., nacre, laminar cross). Secreted polymorph type and microstructural types are used to characterize large mollusk groups, particularly the bivalves.

Nacre is the most studied aragonitic microstructure and is widely distributed in mollusks (*Towe & Hamilton, 1967*). Its stratified microstructure gives mother-of-pearl its luster and provides excellent mechanical properties. Nacre has been of great interest to the pearl industry, making it one of the most studied hard tissues (*Wang et al., 2013*). Because it is osteoconductive and biodegradable, interest has increased recently in technological applications related to nacre, such as the manufacture of bio-inspired super-resistant materials and clinical implants (*Tang et al., 2003; Oaki & Imai, 2005*).

Submitted 10 March 2021

Accepted 6 May 2021

Published 15 July 2021

Corresponding author

Dalila Aldana Aranda,  
daldana@cinvestav.mx

Academic editor

Andrea Scozzafava

Additional Information and  
Declarations can be found on  
page 9

DOI 10.7717/peerj.11527

© Copyright

2021 Santana and Aldana Aranda

Distributed under

Creative Commons CC-BY 4.0

OPEN ACCESS

In each of the three main mollusk classes (Gastropoda, Cephalopoda and Bivalvia) nacre exhibits specific growth patterns and mechanisms. In Gastropoda, for example, the aragonite nanocrystals in the nacre are stacked in towers and their *c* axes are aligned. However, they have a composite cross laminar arrangement, and a third hierarchical order of flat aragonite fibers from 50 to 100 nm thick, 300 nm wide and a few micrometers long (Romana *et al.*, 2013). In the nautilus (Cephalopoda), nacre exhibits a mixed behavior with simultaneous growth in towers and terraces occurring in adjacent locations (Saunders & Landman, 2010). Nacre in the Bivalvia has terraced growth and the three axes of crystals are co-oriented. The order Pterioidea has shells that are unequal, monomyary, and not equilateral; the right valve is generally less convex than the left (Wada & Temkin, 2008; Cummings & Graf, 2015). Their shells are formed by superposition of an outer organic layer, the periostracum, a prismatic layer and the inner nacreous layer (Kennedy, Taylor & Hall, 1969).

Nacre is a biomineral consisting (by weight) of 95% aragonite (CaCO<sub>3</sub>) with the remaining 1–5% being organic matrix (Zhang & Li, 2012). Its microstructure is one of layered “brick” (aragonite tablets) and “mortar” (protein-polysaccharide matrix). This structure provides nacre with twice the strength and up to 1,000 times the toughness of its constituent components alone (Li *et al.*, 2004; Veis & Dorvee, 2013; Morris *et al.*, 2016). Individual nacre tablets have a nanoscale structure based on aragonite nanograins, nanoblocks and nanofibers (Wang *et al.*, 2013). Nanoscale structural organization differs between bivalve mollusks, resulting in different tablet forms at growth completion.

Better understanding of the composition and hierarchy of biological system microstructures is key in the search for new materials and provides deeper insight into evolutionary processes (Jáuregui-Zúñiga *et al.*, 2003; Oaki & Imai, 2005; Wang *et al.*, 2013; Nakamura Filho *et al.*, 2014; Wegst *et al.*, 2015). The present study objective was to analyze the micro- and nanostructure of *P. colymbus* nacre with scanning electron microscopy, and its chemical composition with X-ray diffraction, X-ray fluorescence spectrometry, Fourier transform infrared spectrometry and Raman spectroscopy.

## MATERIALS & METHODS

Shells of *Pteria colymbus* were collected in the Alacranes Reef, in the state of Yucatán, Mexico. They were placed in a soap solution, cleaned, and stored at 4 °C for 48 h. To remove the inorganic and biogenic matter from shells was cleaned by ultrasound with a soap solution for 5 min (Ky, Lo & Planes, 2017). Six 1 cm<sup>2</sup> samples were cut from the shells using a 32 mm-diameter diamond disc. Samples were washed again by ultrasound for five minutes and dried at 65 °C for 3 h (Ren *et al.*, 2009; Xu & Zhang, 2015).

Nacre tablet morphology was characterized with a JEOL 7600F ultra high resolution field emission scanning electron microscope (FESEM). Samples were coated with Au/Pd and processed at a 1–30 kV acceleration voltage (Ren *et al.*, 2009; Liu & Li, 2015).

For the chemical analysis, a 1 cm<sup>2</sup> nacreous layer sample was separated from the shell with the help of a rotary tool at 2000 RPM. The sample was always kept immersed in water at room temperature. The sample was cleaned by ultrasound with a soap solution for five minutes and dried at 65 °C for three hours. Subsequently, it was placed in aluminum

sample holders for analysis in the diffractometer (Bruker D8) using monochromatic CuK $\alpha$  radiation. The XRD patterns were collected at 20–90° (2 $\theta$ ) in 0.02° steps with a 0.96 s count time interval. The resulting diffraction patterns were compared with the card for aragonite (PDF no. 000411475) from the crystallographic records of the International Center for Diffraction Data (ICDD) database (*Weiner & Traub, 1980; De Paula & Silveira, 2009; Heinemann et al., 2011*).

To analyze the nacre by Fourier transform infrared spectrometry (FTIR) analysis, the nacre layer from the shell was separated with a rotary tool at 2000 RPM. The sample was ultrasonically cleaned with a soap solution and dried at 65 °C for 3 h. The sample was ground in an agate mortar to give the appearance of a fine powder and then dried at 65 °C for 3 h. Tablets were prepared with 0.5 mg of nacre powder and 200 mg of KBr. Infrared analyzes were run at a 4 cm resolution in two wave ranges: 400–4,000 cm<sup>-1</sup> and 550–4,000 cm<sup>-1</sup>. The analyzes were done in reflectance mode on a FTIR spectrometer with Bruker accessory (EQUINOX 5). Spectra were automatically corrected for water, carbon dioxide and the KBr background (*Monarumit et al., 2015; Zhang et al., 2016; Cardoso et al., 2016*).

Chemical analyses were also done using the semi-quantitative method of X-ray fluorescence spectrometry (XFR) with wave dispersion in a spectrometer (Bruker S4 Pioneer) with a 4kW excitation source. A vacuum scan was done of 71 elements (11Na-92U) using an RX tube with Rh anode, 25–60 kV excitation voltage, and a 0.46 dg collimator with a 34 mm mask. Data was interpreted with the Spectra Plus software. Quantification of CaCO<sub>3</sub> was done with an ignition loss analysis at 950 °C for 1 h (*Shi et al., 2018*).

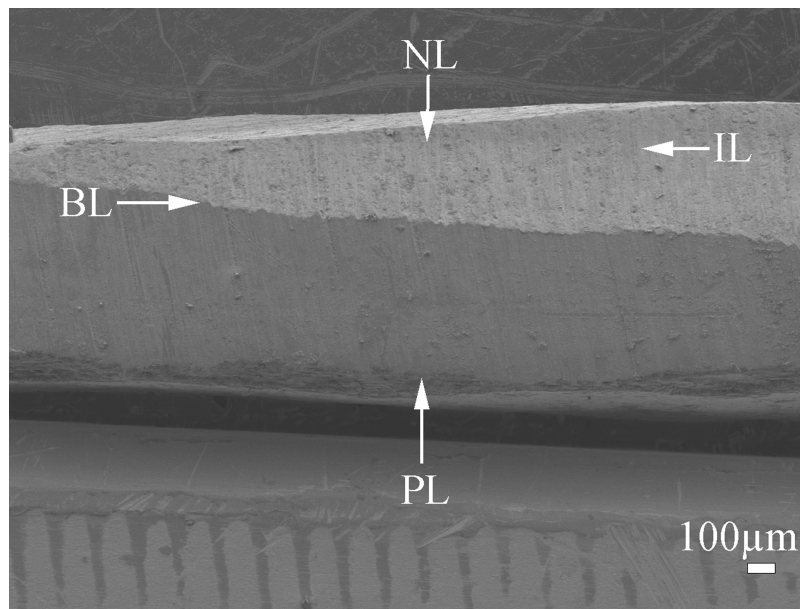
The CaCO<sub>3</sub> crystalline phase was identified using a Raman spectrometer with focal point (WITEC Alpha 300) ( $\lambda_{exc} = 488$  and 785 nm; acquisition time 10 s; resolution 10 cm<sup>-1</sup>).

## RESULTS

### Microstructure and nanostructure

The shell of *P. colymbus* consists of a prismatic and an aragonitic layer clearly divided by a slight change in color (*Fig. 1*, indicated by arrow and BL symbol). The FESEM analysis identified an organic hydrogel on some tablets in different layers (*Fig. 2A*). In another growth section of the pearlescent layer small growing crystals were observed to be fusing with each other (*Fig. 2B*). The tablets form a uniform sheet at the point where the next layer begins to grow and in some cases the tablets fuse with higher layers (*Fig. 2C*). Mature tablets are four to eight-sided, 0.6–3.0  $\mu\text{m}$  in length, and can be fused (*Fig. 2D*).

Cross sections of the nacre tablets showed a nanostructure in which the first layer of deposited nacre consisted of packed nanocrystals forming tablets. These were longer than in the upper layers and their growth was perpendicular to the surface (*Fig. 3A*). Crystals in initial growth stages were observed in a section close to the prismatic layer (*Fig. 3B*). In the intermediate section of the shell all the deposited nacre layers contained tablets composed of a package of crystals fused in the “brick and mortar” arrangement typical of species in the Pteriidae family. Average tablet thickness was 385 nm (SD = 0.069)



**Figure 1** Scanning electron microscopy (SEM) image of the cross-section of *Pteria colymbus* (Mollusca, Bivalvia) shell. General view of pearl oyster *Pteria colymbus* (Mollusca, Bivalvia) shell showing the prismatic layer (PL) at the lower end, followed by the interface zone (BL) and the nacreous layer (NL) at the top. Middle zone of the nacreous layer (IL).

Full-size  DOI: 10.7717/peerj.11527/fig-1

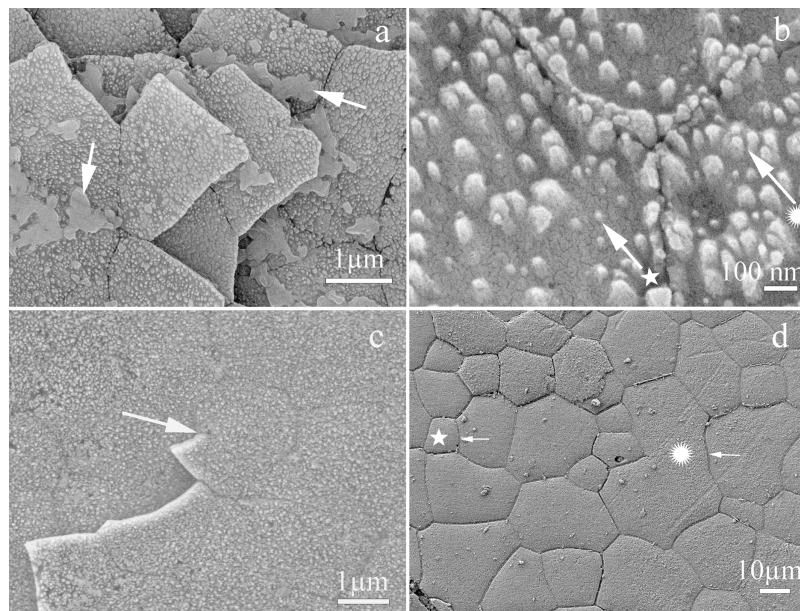
( $n = 187$ ) with a range of 200–530 nm (Fig. 3C). The nanocrystals were uniformly oriented perpendicular to shell surface, have a 41 nm (SD = 9.43) ( $n = 24$ ) average width, and a length range of 24–69 nm ( $n = 24$ ) (Fig. 3D).

### Chemical analysis

The XRD pattern of the nacre layer showed the main reflection to be at 31.05 ( $2\theta$ ) with two lesser readings at 33.0 ( $2\theta$ ) and 66.0 ( $2\theta$ ), both characteristic of aragonite (Fig. 4).

The XRF analysis identified aragonite as representing 98.13% of sample weight. Minor elements were Si (0.72%), Na (0.5500%), S (0.2080%), and Sr (0.1042%), and trace elements were Mg (0.0897%), P (0.0485%), Cu (0.0353%), Al (0.0331), Fe (0.0311%), Cl (0.0290%), K (0.0151%) and Zn (0.0060%). The nacre's aragonite structure was confirmed in the FTIR analysis (Fig. 5). Four bands characteristic of aragonite, corresponding to the  $\text{CO}_3^{2-}$  ions, were identified:  $\nu_3$  at 1,445.96  $\text{cm}^{-1}$ ;  $\nu_1$  at 1,082.72  $\text{cm}^{-1}$ ;  $\nu_2$  at 856.80  $\text{cm}^{-1}$ ; and  $\nu_4$  at 699.81–712.52  $\text{cm}^{-1}$ . The  $\nu_4$  band corresponds to the planar flexion mode of carbonate vibration and the  $\nu_1$  band to the symmetric stretch mode. The nacre FTIR spectrum revealed lower intensity organic bands; the band at 1,786.95  $\text{cm}^{-1}$  was attributed to the carboxylate (carbonyl) groups of the acidic proteins in the organic matrix.

The Raman spectroscopy analysis of the nacre surface produced the most intense band at near 1,085  $\text{cm}^{-1}$  in the aragonite spectra which corresponds to symmetrical stretching mode  $\nu_1$  of the carbonate ion (Fig. 6). Low- to medium-intensity bands in the 100–300  $\text{cm}^{-1}$  region of the aragonite spectra were due to the translational and rotational



**Figure 2** Scanning electron microscopy (SEM) view of the inner surface of the *Pteria colymbus* (Mollusca, Bivalvia) shell. Microstructure of the nacreous tablets in the inner surface of the *Pteria colymbus* shell. The sample did not receive any polishing and etching treatment. (A) Detail of the inner surface of the shell showing recently formed nacre tablets and traces of the hydrogel (arrow) responsible for the formation of the nacre tablets. (B) Detail showing the first stages of nacre crystal formation. Crystal enveloped by organic matrix (★). Crystal in an advanced stage of formation merging with neighboring crystals (☀). (C) Section showing the two different layers of nacre growth merging through a hexagonal-shaped tablet (arrow). (D) Detail of the last layer of nacre showing the different geometries of the nacre tablets. tablet with the minimum number of sides for this species with only 5 μm in length (★). Tablet fused with others with no apparent pattern, which is 40 μm long (☀).

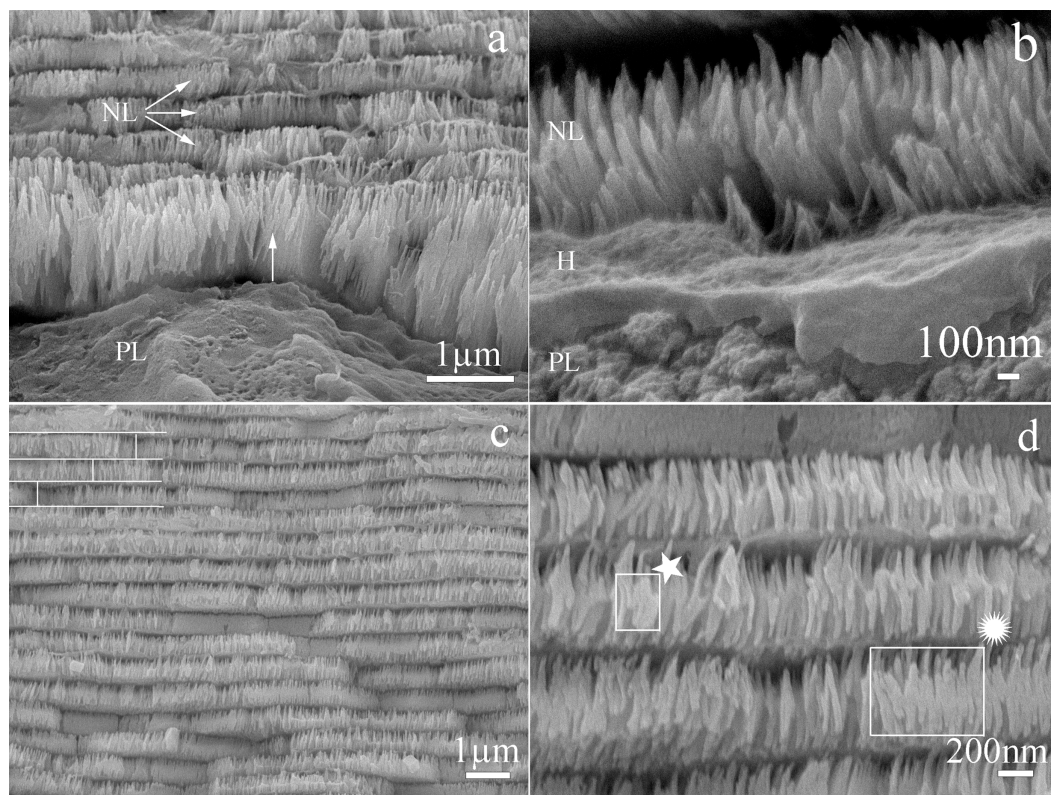
Full-size  DOI: 10.7717/peerj.11527/fig-2

modes of lattice vibration. The  $\nu_4$  in the carbonate ion plane bending mode occurred as a doublet with bands between 701 and 705  $\text{cm}^{-1}$ .

## DISCUSSION

Nacre in *P. colymbus* consists of polygonal tablets with four to eight sides, a morphological characteristic also present in species such as *Pinctada maxima*, *Pinctada radiata* and *Pinctada fucata* (Wang et al., 2001; Bellaaj-Zouari et al., 2011; Zhang, Xie & Yan, 2019). However, tablet length differs between species in the Pteriidae family. In *P. colymbus*, length ranges from 0.6 to 3.0 μm, whereas in *P. radiata* it ranges from 4.0 to 5.0 μm (Bellaaj-Zouari et al., 2011) and in *P. margaritifera* from 5.0 to 10.0 μm (Rousseau et al., 2009).

Morphological differences in pearl oysters can be seasonal or intrinsic to each species (Wada, 1972). Intrinsic differences are due to genetic control of shell mineralogy and any similarities between species can be traced to the Mesozoic/Paleozoic boundary (Kennedy, Taylor & Hall, 1969). Environmental factors such as temperature can modify shell structure in different organisms. For instance, shell aragonite percentage in the mussel *Mytilus californianus* decreases from 45% in the spring to 30% in the winter, but only in organisms longer than 15 mm (Kennedy, Taylor & Hall, 1969). Slower nacre deposition

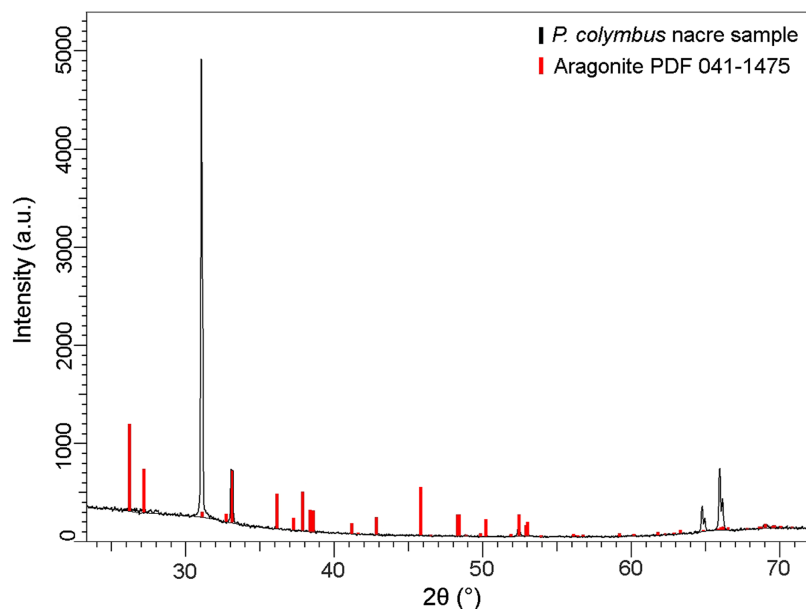


**Figure 3** Scanning electron microscope view of the transverse section of *Pteria colymbus* (Mollusca, Bivalvia) shell. Microstructure of the first and middle nacre layers in the shell of *Pteria colymbus*. (A) Interface zone of the prismatic and nacreous layers. The first layer of nacre crystals has a growth direction perpendicular to the surface (Arrow). The crystals have a greater length compared to the subsequent layers. The next three nacre layers (NL) have better organization and uniform size. (B) Detail of the nacre crystals (NL) in the first stage of growth. The presence of organic hydrogel (H) is observed, which is covering the prismatic layer (PL). (C) Middle zone of the nacre layer. All nacreous layers contain tablets composed of fused individual crystals. The typical brick and mortar formation, typical of bivalve mollusks (represented by white lines) is observed. The average thickness of the tablets was 385 nm (SD = 0.069). (D) Detail of the nacreous layers in the middle zone. The uniform shapes of the tablets are observed, the crystals that make up the tablets show an early stage of growth (★). Crystals merging from the center in the previous layer (⊙). the crystals have a mean width of 41 nm (SD = 9.43).

Full-size [DOI: 10.7717/peerj.11527/fig-3](https://doi.org/10.7717/peerj.11527/fig-3)

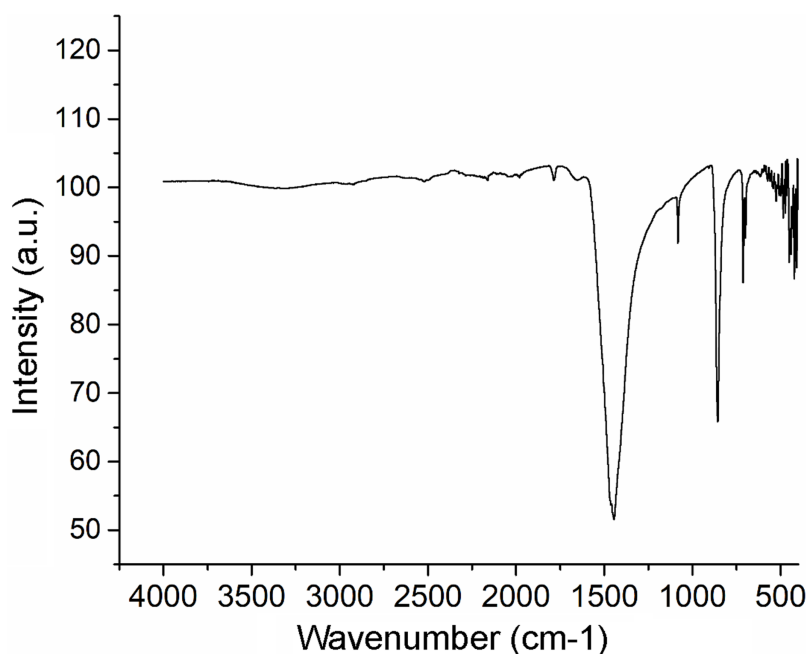
rates may be in response to reductions in water temperature, probably in winter, combined with lower food availability (Taylor & Strack, 2008). In another example, in *P. fucata* nacre growth and thickness respond to tablet thickness which is 324 nm when water temperature is highest, during August, but only 224 nm when it is lower, in December (Muhammad et al., 2017). Decreases in tablet thickness favor light iridescence of the nacre surface which is why pearl producers harvest pearls when sea water temperature decreases (Suzuki & Nagasawa, 2013).

The tablets in *P. colymbus* shell contain nanocrystals ranging in thickness from 24 to 69 nm. This coincides with tablets in *P. maxima* which consist of aragonite nanofibrils from 10 to 30 nm thick (Wang et al., 2013). Tablets in abalone *Haliotis rufescens* shell are built of parallel aragonite nanoparticles (Huang & Li, 2012), and its nanostructure is




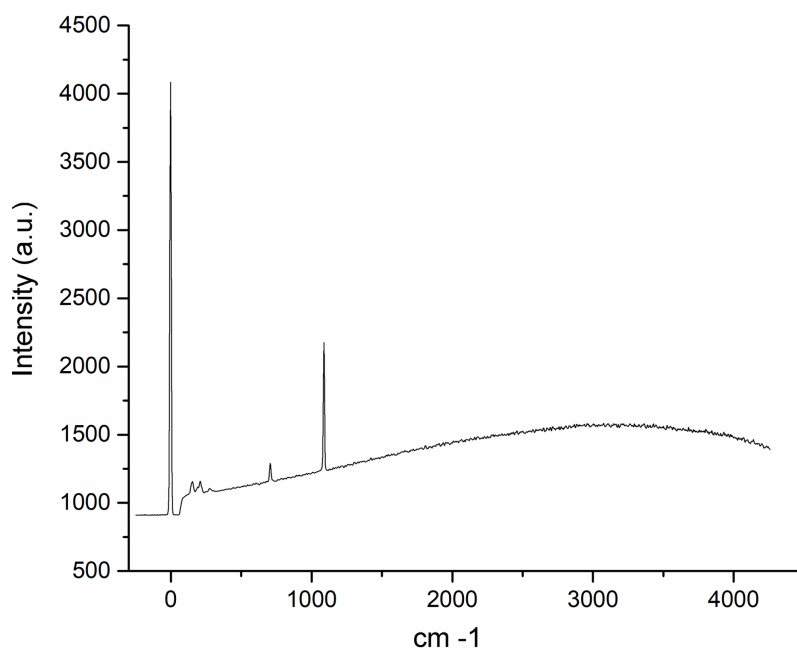
**Figure 4** X-ray diffraction pattern (XRD) of *Pteria colymbus* (Mollusca, Bivalvia) nacre sample. The stronger diffraction peak of aragonite in nacreous layer of *Pteria colymbus* is scanning angle  $2\theta = 31.05^\circ$ . Red bars represent the Aragonite pattern from PDF 041-1475. (For interpretation of the references to color in this figure legend, the reader is referred to the web version of this article).

Full-size  DOI: [10.7717/peerj.11527/fig-4](https://doi.org/10.7717/peerj.11527/fig-4)



**Figure 5** Fourier transform infrared spectrometry (FTIR) spectrum of *Pteria colymbus* (Mollusca, Bivalvia) nacre powder. The nacre powder sample of *Pteria colymbus* displays a characteristic symmetric carbonate stretching vibration ( $\nu_1$ ) at  $1,082.72\text{ cm}^{-1}$  and a carbonate out-of-plane bending vibration ( $\nu_2$ ) at  $856.80\text{ cm}^{-1}$ . The  $\nu_4$  band at  $699.81\text{--}712.52\text{ cm}^{-1}$  corresponds to the planar flexion mode of carbonate vibration.

Full-size  DOI: [10.7717/peerj.11527/fig-5](https://doi.org/10.7717/peerj.11527/fig-5)



**Figure 6** Raman spectra of the *Pteria colymbus* (Mollusca, Bivalvia) nacre layer sample. The nacreous layer of *Pteria colymbus* shows an intense band at near  $1,085\text{ cm}^{-1}$  that corresponds to the symmetrical stretching mode of the carbonate ion. Low- to medium-intensity bands in the  $100\text{--}300\text{ cm}^{-1}$  region were due to the translational and rotational modes of lattice vibration. The carbonate ion plane bending mode occurred as a band between  $701$  and  $705\text{ cm}^{-1}$ . [Full-size !\[\]\(5fd6ef84f97f42d7f8b34275f1b65312\_img.jpg\) DOI: 10.7717/peerj.11527/fig-6](https://doi.org/10.7717/peerj.11527/fig-6)

one of polygonal cobble-like grains ( $\sim 32\text{ nm}$ ) within individual aragonite tablets (*Li et al., 2004*). The shell of *P. fucata* contains nanoblocks from 20 to 180 nm long (*Oaki & Imai, 2005*).

In each species formation of the aragonite nanoparticles in nacre tablets is regulated by organic matrix characteristics (*Dauphin & Denis, 2000; Kim et al., 2006*). The distribution of organic macromolecules during crystal growth is important since these regulate crystal size, shape, and orientation (*Okumura et al., 2012; Shtukenberg, Ward & Kahr, 2017*).

In *Tellinella asperrima* shells, the crystallographic orientation of aragonite between nacre and nacre powder (ground at  $45\text{ }\mu\text{m}$ ) was investigated. It was found that there is a strong preferential crystallographic orientation of the diffraction peak at the angle  $2\theta = 31.03^\circ$  of the intact nacre, simultaneously two other peaks with weak preferential orientations were found (*Ren et al., 2009*). In this work, it was found that the X-ray diffraction pattern of the nacre of *P. colymbus* is very similar to the intact nacre of *T. asperrima*. Presenting greater intensity in the main diffraction peak and the same intensity in the minor peaks. This preferential crystal orientation of aragonite in nacre is frequently found in biological mineralization and is due to the presence of b-chitin fibrils and the protein polypeptide chains that control crystal growth (*Feng et al., 2000*).

Calcium carbonate ( $\text{CaCO}_3$ ) in the form of aragonite represents 98.13% of the total nacre layer in *P. colymbus* in the present results. The majority presence of aragonite in the shell coincides with other species in the Pteriidae family, such as *P. fucata*



(*Saruwatari et al., 2009*) and *P. margaritifera* (*Shi et al., 2018*), as well as the mussel *Perna viridis* (*Xu & Zhang, 2015*). Minor elements are Si, Na, S and Sr, and trace elements are Mg, P, Cu, Al, Fe, Cl, K and Zn. In another study, nacre was found to be composed of calcium carbonate (91.50%) with traces of organic substances (3.83%), residual substances (0.01%) and water (3.97%) (*Taylor & Strack, 2008*). These residual substances include Na, Cl and K, as well as traces and other elements such as Ba, Mg, P, Mn, Fe, Al, Cu, Zn, Ag, Hg, Li and Mr. The trace element profile of a nacre reflects water mineral composition in the place where it formed. In biogenic aragonite crystals other elements such as Mn, Mg, Sr and Ba can substitute for calcium (*Gaetani & Cohen, 2006; Chen et al., 2011*). Notable differences in the concentration of these elements exist between taxonomic groups, highlighting genetic influence on their incorporation (*Carré et al., 2006*).

The other elements present in nacre function as precursor ions in nacre formation, as catalysts in proteins and activators of enzymes; they are present in intercrystalline organic macromolecules and the organism's epithelial fluid (*Marsh & Sass, 1983; Cho & Jeong, 2011; Marin, 2012*).

## CONCLUSIONS

Nacre composition in *P. colymbus* has high aragonite content and its nanostructure consists of polygonal tablets built of nanocrystals. The present is a preliminary description of *P. colymbus* shell structure intended as a presentation of the relevant data to date, and a guide for further research.

## ACKNOWLEDGEMENTS

The authors thank Patricia Quintana access to LANNBIO facilities, Dora Huerta, and Daniel Aguilar for assistance with the diffractograms and SEM images. The authors also thank Maria del Socorro Garcia Guillermo, Ixchel Rubí Perez, Ana Elena Muñoz, and Norma Alicia Berlanga, at Cinvestav-Salttillo chemical analysis General Laboratory for her support in carrying out this work.

## ADDITIONAL INFORMATION AND DECLARATIONS

### Funding

The research reported here was financed in part by the Consejo Nacional de Ciencia y Tecnología (Grant No. CVU 390072). X-ray diffraction and SEM analyses were done at the National Laboratory of Nano- and Biomaterials (LANNBIO), CINVESTAV-IPN Unidad Merida, and funded by the Fomix-Yucatán and CONACyT (Grant No. 2008–108160 Y). The funders had no role in study design, data collection and analysis, decision to publish, or preparation of the manuscript.

### Grant Disclosures

The following grant information was disclosed by the authors:  
Consejo Nacional de Ciencia y Tecnología: CVU 390072.  
National Laboratory of Nano- and Biomaterials (LANNBIO).

CINVESTAV-IPN Unidad Merida.  
Fomix-Yucatán and CONACyT: 2008–108160 Y.

### Competing Interests

The authors declare that they have no competing interests.

### Author Contributions

- Pablo Santana conceived and designed the experiments, performed the experiments, analyzed the data, prepared figures and/or tables, authored or reviewed drafts of the paper, and approved the final draft.
- Dalila Aldana Aranda conceived and designed the experiments, performed the experiments, analyzed the data, prepared figures and/or tables, authored or reviewed drafts of the paper, and approved the final draft.

### Data Availability

The following information was supplied regarding data availability:

Raw measurements are available in [Supplemental File](#).

### Supplemental Information

Supplemental information for this article can be found online at <http://dx.doi.org/10.7717/peerj.11527#supplemental-information>.

## REFERENCES

- Addadi L, Raz S, Weiner S. 2003.** Taking advantage of disorder: amorphous calcium carbonate and its roles in biomineralization. *Advanced Materials* **15**(12):959–970  
DOI [10.1002/adma.200300381](https://doi.org/10.1002/adma.200300381).
- Bellaaj-Zouari A, Chérif K, Elloumi-Hannachi I, Slimane N, Habib J. 2011.** Characterization of mineral and organic phases in nacre of the invasive pearl oyster *Pinctada radiata* (Leach, 1814). *Cahiers de Biologie Marine* **52**:337–348.
- Cardoso SSS, Cartwright JHE, Checa AG, Sainz-Díaz CI. 2016.** Fluid-flow-templated self-assembly of calcium carbonate tubes in the laboratory and in biomineralization: the tubules of the watering-pot shells, Clavagelloidea. *Acta Biomaterialia* **43**:338–347  
DOI [10.1016/j.actbio.2016.07.005](https://doi.org/10.1016/j.actbio.2016.07.005).
- Carré M, Bentaleb I, Bruguier O, Ordinola E, Barrett NT, Fontugne M. 2006.** Calcification rate influence on trace element concentrations in aragonitic bivalve shells: evidences and mechanisms. *Geochimica et Cosmochimica Acta* **70**(19):4906–4920  
DOI [10.1016/j.gca.2006.07.019](https://doi.org/10.1016/j.gca.2006.07.019).
- Chen T, Yu K, Li S, Chen T, Shi Q. 2011.** Anomalous Ba/Ca signals associated with low temperature stresses in Porites corals from Daya Bay, northern South China Sea. *Journal of Environmental Sciences* **23**(9):1452–1459 DOI [10.1016/S1001-0742\(10\)60606-7](https://doi.org/10.1016/S1001-0742(10)60606-7).
- Cho S-M, Jeong W-G. 2011.** Prismatic shell repairs by hemocytes in the extrapallial fluid of the Pacific Oyster, *Crassostrea gigas*. *The Korean Journal of Malacology* **27**(3):223–228  
DOI [10.9710/kjm.2011.27.3.223](https://doi.org/10.9710/kjm.2011.27.3.223).
- Cummings KS, Graf DL. 2015.** Class Bivalvia. In: *Thorp and Covich's Freshwater Invertebrates*. Amsterdam: Elsevier, 423–506.

- Dauphin Y, Denis A. 2000.** Structure and composition of the aragonitic crossed lamellar layers in six species of Bivalvia and Gastropoda. *Comparative Biochemistry and Physiology Part A: Molecular & Integrative Physiology* **126**(3):367–377 DOI [10.1016/S1095-6433\(00\)00213-0](https://doi.org/10.1016/S1095-6433(00)00213-0).
- De Paula SM, Silveira M. 2009.** Studies on molluscan shells: contributions from microscopic and analytical methods. *Micron* **40**(7):669–690 DOI [10.1016/j.micron.2009.05.006](https://doi.org/10.1016/j.micron.2009.05.006).
- Feng QL, Cui FZ, Pu G, Wang RZ, Li HD. 2000.** Crystal orientation, toughening mechanisms and a mimic of nacre. *Materials Science and Engineering C* **11**:19–25 DOI [10.1016/S0928-4931\(00\)00138-7](https://doi.org/10.1016/S0928-4931(00)00138-7).
- Gaetani GA, Cohen AL. 2006.** Element partitioning during precipitation of aragonite from seawater: a framework for understanding paleoproxies. *Geochimica et Cosmochimica Acta* **70**(18):4617–4634 DOI [10.1016/j.gca.2006.07.008](https://doi.org/10.1016/j.gca.2006.07.008).
- Heinemann F, Launspach M, Gries K, Fritz M. 2011.** Gastropod nacre: structure, properties and growth—biological, chemical and physical basics. *Biophysical Chemistry* **153**(2–3):126–153 DOI [10.1016/j.bpc.2010.11.003](https://doi.org/10.1016/j.bpc.2010.11.003).
- Huang Z, Li X. 2012.** Order-Disorder Transition of Aragonite Nanoparticles in Nacre. *Physical Review Letters* **109**:025501 DOI [10.1103/PhysRevLett.109.025501](https://doi.org/10.1103/PhysRevLett.109.025501).
- Jáuregui-Zúñiga D, Reyes-Grajeda JP, Sepúlveda-Sánchez JD, Whitaker JR, Moreno A. 2003.** Crystallochemical characterization of calcium oxalate crystals isolated from seed coats of *Phaseolus vulgaris* and leaves of *Vitis vinifera*. *Journal of Plant Physiology* **160**(3):239–245 DOI [10.1078/0176-1617-00947](https://doi.org/10.1078/0176-1617-00947).
- Kennedy WJ, Taylor JD, Hall A. 1969.** Environmental and biological controls on bivalve shell mineralogy. *Biological Reviews* **44**(4):499–530 DOI [10.1111/j.1469-185X.1969.tb00610.x](https://doi.org/10.1111/j.1469-185X.1969.tb00610.x).
- Kim Y-Y, Catino JW, Tomaino GP, Cox SD. 2006.** Bio-Inspired Hydrogel-Calcium Carbonate Core-Shell Particles. *MRS Online Proceedings Library (OPL)* 988 DOI [10.1557/PROC-988-0988-QQ03-04](https://doi.org/10.1557/PROC-988-0988-QQ03-04).
- Ky C-L, Lo C, Planes S. 2017.** Mono- and polychromatic inner shell phenotype diversity in *Pinctada margaritifera* donor pearl oysters and its relation with cultured pearl colour. *Aquaculture* **468**(2):199–205 DOI [10.1016/j.aquaculture.2016.10.017](https://doi.org/10.1016/j.aquaculture.2016.10.017).
- Li X, Chang W-C, Chao YJ, Wang R, Chang M. 2004.** Nanoscale structural and mechanical characterization of a natural nanocomposite material: the shell of red abalone. *Nano Letters* **4**(4):613–617 DOI [10.1021/nl049962k](https://doi.org/10.1021/nl049962k).
- Liu X, Li J. 2015.** Formation of the prismatic layer in the freshwater bivalve *Hyriopsis cumingii*: the feedback of crystal growth on organic matrix. *Acta Zoologica* **96**(1):30–36 DOI [10.1111/azo.12048](https://doi.org/10.1111/azo.12048).
- Marin F. 2012.** The formation and mineralization of mollusk shell. *Frontiers in Bioscience* **S4**(3):1099–1125 DOI [10.2741/s321](https://doi.org/10.2741/s321).
- Marsh ME, Sass RL. 1983.** Calcium-binding phosphoprotein particles in the extrapallial fluid and innermost shell lamella of clams. *Journal of Experimental Zoology* **226**(2):193–203 DOI [10.1002/jez.1402260204](https://doi.org/10.1002/jez.1402260204).
- Monarumit N, Noirawee N, Phlayrahan A, Promdee K, Won-in K, Satitkune S. 2015.** Identification of high-luster and lusterless freshwater-cultured pearls by X-ray absorption spectroscopy. *Journal of Applied Spectroscopy* **82**(4):677–680 DOI [10.1007/s10812-015-0163-3](https://doi.org/10.1007/s10812-015-0163-3).
- Morris JP, Wang Y, Backeljau T, Chapelle G. 2016.** Biomimetic and bio-inspired uses of mollusc shells. *Marine Genomics* **27**:85–90 DOI [10.1016/j.margen.2016.04.001](https://doi.org/10.1016/j.margen.2016.04.001).
- Muhammad G, Atsumi T, Sunardi, Komaru A. 2017.** Nacre growth and thickness of Akoya pearls from Japanese and Hybrid *Pinctada fucata* in response to the aquaculture temperature condition in Ago Bay, Japan. *Aquaculture* **477**(1–2):35–42 DOI [10.1016/j.aquaculture.2017.04.032](https://doi.org/10.1016/j.aquaculture.2017.04.032).

- Nakamura Filho A, De Almeida AC, Riera HE, De Araújo JLF, Gouveia VJP, De Carvalho MD, Cardoso AV. 2014. Polymorphism of CaCO<sub>3</sub> and microstructure of the shell of a Brazilian invasive mollusc (*Limnoperna fortunei*). *Materials Research* 17(Suppl. 1):15–22 DOI 10.1590/S1516-14392014005000044.
- Oaki Y, Imai H. 2005. The hierarchical architecture of nacre and its mimetic material. *Angewandte Chemie International Edition* 44(40):6571–6575 DOI 10.1002/anie.200500338.
- Okumura T, Suzuki M, Nagasawa H, Kogure T. 2012. Microstructural variation of biogenic calcite with intracrystalline organic macromolecules. *Crystal Growth & Design* 12(1):224–230 DOI 10.1021/cg200947c.
- Ren F, Wan X, Ma Z, Su J. 2009. Study on microstructure and thermodynamics of nacre in mussel shell. *Materials Chemistry and Physics* 114(1):367–370 DOI 10.1016/j.matchemphys.2008.09.036.
- Romana L, Thomas P, Bilas P, Mansot JL, Merrifields M, Bercion Y, Aranda DA. 2013. Use of nanoindentation technique for a better understanding of the fracture toughness of *Strombus gigas* conch shell. *Materials Characterization* 76:55–68 DOI 10.1016/j.matchar.2012.11.010.
- Rousseau M, Meibom A, Gèze M, Bourrat X, Angellier M, Lopez E. 2009. Dynamics of sheet nacre formation in bivalves. *Journal of Structural Biology* 165(3):190–195 DOI 10.1016/j.jsb.2008.11.011.
- Saruwatari K, Matsui T, Mukai H, Nagasawa H, Kogure T. 2009. Nucleation and growth of aragonite crystals at the growth front of nacles in pearl oyster, *Pinctada fucata*. *Biomaterials* 30(16):3028–3034 DOI 10.1016/j.biomaterials.2009.03.011.
- Saunders WB, Landman NH. 2010. *Nautilus: the biology and paleobiology of a living fossil, reprint with additions*. Dordrecht, Netherlands: Springer.
- Shi L, Wang Y, Liu X, Mao J. 2018. Component analysis and identification of Black Tahitian cultured pearls from the oyster *Pinctada margaritifera* using Spectroscopic Techniques. *Journal of Applied Spectroscopy* 85(1):98–102 DOI 10.1007/s10812-018-0618-4.
- Shtukenberg AG, Ward MD, Kahr B. 2017. Crystal growth with macromolecular additives. *Chemical Reviews* 117(24):14042–14090 DOI 10.1021/acs.chemrev.7b00285.
- Suzuki M, Nagasawa H. 2013. Mollusk shell structures and their formation mechanism. *Canadian Journal of Zoology* 91(6):349–366 DOI 10.1139/cjz-2012-0333.
- Tang Z, Kotov NA, Magonov S, Ozturk B. 2003. Nanostructured artificial nacre. *Nature Materials* 2(6):413–418 DOI 10.1038/nmat906.
- Taylor J, Strack E. 2008. Pearl oroduction. In: *The Pearl Oyster*. Amsterdam: Elsevier, 273–302.
- Towe KM, Hamilton GH. 1967. Ultrastructure and inferred calcification of the mature and developing nacre in bivalve mollusks. *Calcified Tissue Research* 1(1):306–318 DOI 10.1007/BF02008102.
- Veis A, Dorvee JR. 2013. Biomineralization mechanisms: a new paradigm for crystal nucleation in organic matrices. *Calcified Tissue International* 93(4):307–315 DOI 10.1007/s00223-012-9678-2.
- Wada K. 1972. Nucleation and growth of aragonite crystals in the nacre of bivalve molluscs. *Biomineralization* 6:141–159.
- Wada KT, Tëmkin I. 2008. Chapter 2—taxonomy and phylogeny. In: Southgate PC, Lucas JS, eds. *The Pearl Oyster*. London: Elsevier, 37–75.
- Wang RZ, Suo Z, Evans AG, Yao N, Aksay IA. 2001. Deformation mechanisms in nacre. *Journal of Materials Research* 16(9):2485–2493 DOI 10.1557/JMR.2001.0340.

- Wang S-N, Yan X-H, Wang R, Yu D-H, Wang X-X. 2013.** A microstructural study of individual nacre tablet of *Pinctada maxima*. *Journal of Structural Biology* **183**(3):404–411 DOI [10.1016/j.jsb.2013.07.013](https://doi.org/10.1016/j.jsb.2013.07.013).
- Wegst UGK, Bai H, Saiz E, Tomsia AP, Ritchie RO. 2015.** Bioinspired structural materials. *Nature Materials* **14**(1):23–36 DOI [10.1038/nmat4089](https://doi.org/10.1038/nmat4089).
- Weiner S, Traub W. 1980.** X-ray diffraction study of the insoluble organic matrix of mollusk shells. *FEBS Letters* **111**(2):311–316 DOI [10.1016/0014-5793\(80\)80817-9](https://doi.org/10.1016/0014-5793(80)80817-9).
- Xu J, Zhang G. 2015.** Unique morphology and gradient arrangement of nacre's platelets in green mussel shells. *Materials Science and Engineering: C* **52**:186–193 DOI [10.1016/j.msec.2015.03.051](https://doi.org/10.1016/j.msec.2015.03.051).
- Zhang G, Li X. 2012.** Uncovering aragonite nanoparticle self-assembly in nacre—a natural armor. *Crystal Growth & Design* **12**(9):4306–4310 DOI [10.1021/cg3010344](https://doi.org/10.1021/cg3010344).
- Zhang R, Xie L, Yan Z. 2019.** *Biomineralization mechanism of the pearl oyster, pinctada fucata*. Singapore: Springer.
- Zhang N, Yang S, Xiong L, Hong Y, Chen Y. 2016.** Nanoscale toughening mechanism of nacre tablet. *Journal of the Mechanical Behavior of Biomedical Materials* **53**(08):200–209 DOI [10.1016/j.jmbbm.2015.08.020](https://doi.org/10.1016/j.jmbbm.2015.08.020).